

# Aggregated functional data model for Near-Infrared Spectroscopy calibration and prediction

Ronaldo Dias, Nancy L. Garcia\*, Guilherme Ludwig  
University of Campinas, BRAZIL

and Marley A. Saraiva  
Federal University of Goiás, BRAZIL

September 3, 2018

## Abstract

Calibration and prediction for NIR spectroscopy data are performed based on a functional interpretation of the Beer-Lambert formula. Considering that, for each chemical sample, the resulting spectrum is a continuous curve obtained as the summation of overlapped absorption spectra from each analyte plus a Gaussian error, we assume that each individual spectrum can be expanded as a linear combination of B-splines basis. Calibration is then performed using two procedures for estimating the individual analytes curves: basis smoothing and smoothing splines. Prediction is done by minimizing the square error of prediction. To assess the variance of the predicted values, we use a leave-one-out jackknife technique. Departures from the standard error models are discussed through a simulation study, in particular, how correlated errors impact on the calibration step and consequently on the analytes' concentration prediction. Finally, the performance of our methodology is demonstrated through the analysis of two publicly available datasets.

**Key words:** B-splines, leave-one-out jackknife, square error of prediction.

**AMS Classification:** Primary: 62G08; Secondary: 92E99.

---

\*Corresponding author: [nancy@ime.unicamp.br](mailto:nancy@ime.unicamp.br)

# 1 Introduction

Different substances reflect light in a characteristic way. The ultraviolet light has wavelength (in nanometers) in the range 1 – 400 nm, visible light in 400–750 nm and infrared region in 750 to  $10^6$  nm. The latter is subdivided into near-infrared (NIR) region: 750–2500 nm, mid-infrared (MIR) region: 2500–16,000 nm and far-infrared (FIR): 16,000– $10^6$  nm. When materials are submitted to different wavelengths, the overtones and combinations in the NIR band will produce very complex patterns that characterize the constituents of the sample. Usually the samples are submitted to different wavelengths of intervals of less than 10 nm and the spectrum is a curve, although it is only measured at discrete set of points. Hence, the different characteristic curves of the constituents of the sample overlap and give rise to a curve which is a sum of several curves depending on the concentration of each substance.

There are several techniques to measure the constituents of a sample. As expected, the very precise are expensive, so-called analytical techniques, while others are relatively inexpensive at the cost of precision, as in the case of NIR spectroscopy. Inexpensive techniques usually require an “instrument calibration” step. Let us begin with a quote regarding NIR spectroscopy: “Near-infrared (NIR) spectroscopy is a technique whose time has arrived. And for good reason: it is unusually fast compared to other analytical techniques (often taking less than 30 seconds), it is non-destructive, and as often as not no sample preparation is required. It is also remarkably versatile. If samples contain such bonds as C-H, N-H, or O-H, and if the concentration of the analyte exceeds about 0.1% of the total composition, then it is very likely to yield acceptable answers – even in the hands of relatively untrained personnel. The price to be paid, however, is the preliminary work, typical of any chemometric method. The instrument/computer system must be “taught” what is important in the sample” (Burns and Ciurczak, 2007). Literature is filled with practical applications of NIR spectroscopy such as food safety testing, protein detection, pharmaceutical development, forensics, to mention just a few. For introductory material on the subject see Shenk and Westerhaus (1991), Davis (2000), Siesler, Ozaki, Kawata and Heise (2002), Brereton (2003) and Burns and Ciurczak (2007).

For practical reasons, it is only possible to measure the spectral data at a finite number of wavelengths  $t_1 < t_2 < \dots < t_T$ . Often  $T$  is in the range 100–200 or even more. For this reason, these data are generally analyzed with multivariate data analysis techniques (multiple linear

regression (MLR), principal components regression (PCR) and partial least squares (PLS), see Brereton, 2003) which consider the spectrum as a set of  $T$  different variables. In this case, the ordering of the wavelengths is irrelevant and correlation among close points is not included in the model. From an experimenter point of view it could be more informative to describe the spectrum as function rather than as set of points, hereby taking into account the physical background of the spectrum, being the sum of absorption peaks for the different chemical components, whose absorbance at wavelengths close to each other are highly correlated. In addition, an important advantage of the functional data analysis approach is to allow measurements to be taken at different wavelengths for each calibration sample as well as for the prediction samples a situation that cannot be treated with the usual multivariate methods.

The objective of this work is to propose a functional model to analyze this data, based on an application of the Beer-Lambert law. The proposed framework is to assume that each absorbance function is a smooth curve that can be well approximated by a function belonging to a finite dimensional space  $\mathcal{H}_K$  which is spanned by  $K$  (fixed) basis functions, in this case B-splines. See, for example, Silverman (1986), Kooperberg and Stone (1991), Vidakovic (1999), Dias (1999). Although this fact might lead one to think that the non-parametric problem becomes a parametric problem, one notices that the number of coefficients can be as large as the number of observations, the smoothing will be obtained by a penalization criteria with the penalizing factor chosen by cross-validation (Wahba, 1990).

The idea of viewing the spectra as a continuous function was proposed by Alsberg (1993). Since then, several papers have been written on the subject of non-parametric estimation of NIR spectroscopy data, ranging from Neural Networks, Support Vector Machine techniques, smoothing splines, kernel approximation among others. We refer the interested reader to the book of Ferraty and Vieu (2006) and references therein. Nevertheless, we agree with the view of Saeys, De Ketelaere, and Darius (2008) that the potential of functional data analysis has not been grasped by most of practitioners. Differently from the commonly used techniques, this paper presents a non-parametric model-based approach that can be easily implemented and analyzed and not only works for prediction but also provides the individual calibration curves for each analyte. This disaggregation of the spectra leads to new developments such as jointly calibration and prediction and outlier prediction to be addressed in future work.

In this work we analyze two artificial datasets, one with strongly correlated measurement

errors and another just weakly correlated to demonstrate the impact of correlation in the calibration step of the analysis. Borggaard and Thodberg (1992) cite the correlation as an important issue in the analysis of spectra, since the fine sampling usually results in large correlation between adjacent points in the spectrum. Also, we apply the non-parametric analysis to two real datasets. The first dataset consists of the absorbance curves of polyaromatic hydrocarbons presented in the textbook by Brereton (2003) to illustrate multivariate calibration and prediction techniques. This is an interesting sample to analyze since it was designed to achieve an orthogonal design in the calibration step. It was also analyzed, using a Bayesian perspective, but only for the calibration step, by Dias, Garcia and Schmidt (2012). The other one is the so-called Tecator Data which is used by several authors to compare the techniques in terms of prediction tool, for example in the works by Borggaard and Thodberg (1992), Eilers, Li and Marx (2009), Ferraty and Vieu (2006), Aneiros-Pérez and Vieu (2006).

This work is organized as follows: Section 2 discusses the suitability of the aggregated functional data model for the spectroscopy data. Sections 3 and 4 show how the calibration and the prediction step, respectively, are performed. We used simulated datasets with different degrees of complexity (Section 5) as well as real data sets taken from Jørgensen and Goegebeur (2007) (Section 6). All estimation procedures were made using the software R, by R Development Core Team (2010). The computer code is available from the authors upon request.

## 2 The model: Beer-Lambert law

A chemical sample is a compound of several *constituents*. A pure chemical sample would be composed of only one constituent. Each constituent of interest is called an *analyte*, the amount of the analyte  $\ell$  is called  $y_\ell$ ,  $\ell = 1, \dots, m$ . A sample is called *closed* if  $y_1 + \dots + y_m = 1$ , i.e. when all constituents in the compound are analyzed. It is very uncommon to work with closed samples. In this work, we will assume that only a subset of constituents is considered.

The term *spectral data* refers to the absorbances  $W(t_1), \dots, W(t_T)$  measured at  $T$  wavelengths  $t_1 < t_2 < \dots < t_T$ . The Beer-Lambert law for one sample considering  $m$  analytes is the linear relationship between absorbance and concentration of the analytes given by

$$W(t) = \theta_0(t) + \sum_{\ell=1}^m y_\ell \theta_\ell(t) + \epsilon(t), \quad (2.1)$$

with the restriction

$$\sum_{\ell=1}^m \theta_{\ell}(t) = 0, \quad (2.2)$$

for  $t = t_1, \dots, t_T$ .

In this work, we consider that expression (2.1) is true for all wavelengths in an appropriate interval  $[A, B]$  with  $\epsilon(t)$  being a Gaussian process with covariance function given by  $\sigma(s, t) = \text{Cov}(\epsilon(s), \epsilon(t))$ .

We shall restrict ourselves to expand the absorbance curves in the well-known cubic B-splines basis. That is, there exist a positive integer  $K$  and a knot sequence  $\xi_1 \leq \dots \leq \xi_{K+4}$  such that

$$\theta_{\ell}(t) = \sum_{k=1}^K \beta_{\ell,k} B_k(t), \quad (2.3)$$

where  $B_k(t)$ ,  $k = 1, \dots, K$  are cubic B-splines. More precisely, the  $k$ -th B-spline of order  $r$  for the knot sequence  $\xi_1, \dots, \xi_{K+r}$  is defined by

$$B_k(t) = (\xi_{k+r} - \xi_k)[\xi_k, \dots, \xi_{k+r}](\xi_k - t)_+^{r-1} \quad \text{for all } t \in \mathbb{R},$$

where  $[\xi_k, \dots, \xi_{r+k}](\xi_k - t)_+^{r-1}$  is  $r$ th divided difference of the function  $(\xi_k - t)_+^{r-1}$  evaluated at points  $\xi_k, \dots, \xi_{r+k}$ . For more details see de Boor (1978). Moreover, B-splines have an important computational property, they are splines with smallest possible support. In other words, B-splines are zero on a large set. Furthermore, a stable evaluation of B-splines with the aid of a recurrence relation is possible.

The model (2.1) can therefore be rewritten as

$$W(t) = \sum_{k=1}^K \left[ \beta_{0,k} + \sum_{\ell=1}^m y_{\ell} \beta_{\ell,k} \right] B_k(t) + \epsilon(t) \quad (2.4)$$

where  $B_k(t)$  corresponds to the  $k$ -th B-spline basis evaluated at  $t$  and  $\beta_{\ell,k}$  is the corresponding coefficient for the  $\ell$ -th constituent.

### 3 Calibration Procedure

First we are going to propose a procedure for *calibration* using the approach of functional data analysis. The calibration problem can be thought as a supervised learning procedure. Assume we are given  $I$  samples of varying compositions. Therefore, our data consists of  $I$  spectra

measured by NIR instrument  $W_i(t), i = 1, \dots, I$ , observed at a finite set of wavelengths. For simplicity, we are going to consider that all of them were observed at the same wavelengths  $t = t_1, \dots, t_T$ , but this assumption is not necessary. Also, we are given a matrix  $Y$  with linear independent lines containing the concentrations measured by a reference method  $y_{i,\ell}$  for  $i = 1, \dots, I$  and  $\ell = 1, \dots, m$ . We are going to assume that the curves  $W(\cdot)$  are smooth functions that are observed at discrete points and we are going to use a functional form of the Beer-Lambert equation. Calibration methods study how  $Y$  varies with  $W$ . That is, given the model (2.1), how do we estimate the functions  $\theta_\ell(t), \ell = 0, 1, \dots, m$ .

The interesting feature of (2.4) restricted to the observed points is that it can be seen as a linear model,

$$\mathbf{W} = \mathbf{X}\boldsymbol{\beta} + \boldsymbol{\varepsilon},$$

where  $\boldsymbol{\beta}$  contains the parameters  $\beta_{\ell,k}, \ell = 0, \dots, m, k = 1, \dots, K$  to be estimated,  $\boldsymbol{\varepsilon}$  represents the error vector,  $\mathbf{W}$  is a stacked vector containing the  $I$  observed spectra at the points  $t_1, \dots, t_T$ ,  $\mathbf{X}$  contains the suitable linear coefficients, that can be written as  $\mathbf{X} = (\mathbf{1}_{n \times 1} \mid \mathbf{Y}) \otimes \mathbf{B}$ , where  $\otimes$  is the Kronecker matrix product and  $\mathbf{B}$  an ordinary B-spline design matrix. The restriction (2.2) is included into the model, in the way suggested by Ramsay and Silverman (2005) to avoid a constrained optimization step: an additional vector of zeros, with length  $T$ , is appended to the observed  $\mathbf{W}$ , and the row vector  $(0 \mid \mathbf{1}_{1 \times m})$  is appended beneath the matrix  $(\mathbf{1}_{I \times 1} \mid \mathbf{Y})$ . The expanded model is

$$\begin{pmatrix} \mathbf{W}_{IT \times 1} \\ \mathbf{0}_{T \times 1} \end{pmatrix} = \left( \left( \begin{array}{c|c} \mathbf{1}_{I \times 1} & \mathbf{Y}_{I \times m} \\ \hline 0 & \mathbf{1}_{1 \times m} \end{array} \right) \otimes \mathbf{B} \right) \boldsymbol{\beta} + \boldsymbol{\varepsilon}. \quad (3.5)$$

In this work we are going to consider two procedures for estimation:

- (a) **Basis smoothing:** In this case  $K$  will be chosen in an *ad-hoc* manner suitable for estimating local features of the curves but also small enough to guarantee the required degree of smoothness. In this case, the coefficient vector  $\boldsymbol{\beta}$  can be obtained as the ordinary least squares estimate, ignoring correlation which yields the explicit solution

$$\hat{\boldsymbol{\beta}} = (\mathbf{X}^+ \mathbf{X}^+)^{-1} \mathbf{X}^+ \mathbf{W}^+, \quad (3.6)$$

in which  $\mathbf{X}^+$  and  $\mathbf{W}^+$  are  $\mathbf{X}$  and  $\mathbf{W}$  augmented with zeros as in equation (3.5).

- (b) **Smoothing splines:** Here we are going to use every observation point as a knot, getting therefore a number of coefficients to be estimated as large as the number of observations. To achieve the desired smoothness we apply a penalty to the squared norm of the second derivative of the spline basis in the least squares problem

$$(\mathbf{W}^+ - \mathbf{X}^+ \boldsymbol{\beta})' (\mathbf{W}^+ - \mathbf{X}^+ \boldsymbol{\beta}) + \lambda \boldsymbol{\beta}' (\mathbf{I}_{m \times m} \otimes \mathbf{R}) \boldsymbol{\beta}$$

which yields the solution

$$\hat{\boldsymbol{\beta}} = (\mathbf{X}^{+'} \mathbf{X}^+ + \lambda \mathbf{I}_{m \times m} \otimes \mathbf{R})^{-1} \mathbf{X}^{+'} \mathbf{W}^+,$$

where  $\mathbf{R}$  is a matrix with entries  $\mathbf{R}_{i,j} = \int_{-\infty}^{\infty} D^2 B_i(t) D^2 B_j(t) dt$ , and  $D^2$  is the second order differential operator  $\partial^2 / \partial t^2$ . The degree of smoothness will be controlled either by inspection of the curves plots (which will be referred to as an “eyeballing method”) or by minimization of the generalized cross-validation criteria (GCV, see Wahba (1990)). Notice particularly that the minimum GCV for all analytes is not achieved by the minimization of the observed aggregated curves, due to the triangle inequality

$$\left\| D^2 \sum_{\ell=0}^m y_{i,\ell} \theta_{\ell}(t) \right\|^2 \leq \sum_{\ell=0}^m |y_{i,\ell}| \left\| D^2 \theta_{\ell}(t) \right\|^2,$$

where  $\|\cdot\|$  is the functional norm. This implies that the optimality of GCV based choices of  $\lambda$  in ordinary smoothing problems cannot be extended to this calibration context, which leaves eyeballing as an equally valid choice.

## 4 Prediction

Once we have the estimated analyte absorbance curves  $\hat{\theta}_{\ell}(t)$ ,  $\ell = 0, \dots, m$ , we can proceed to perform *prediction*, the second step of the analysis. At this point, we are given a new set of  $J$  spectra measured by the same NIR instrument,  $W_j^*(t)$ ,  $j = 1, \dots, J$ , all of them observed at the wavelengths  $t = t_1, \dots, t_T$  (for the sake of simplicity we maintain the same notation but the measured points for prediction can be distinct from the ones used for calibration). Using this new set of data, we want to predict now the new concentrations  $y_{j,\ell}^*$  using the Beer-Lambert relationship

$$W_j^*(t) = \sum_{k=1}^K \left[ \beta_{0,k} + \sum_{\ell=1}^m \beta_{\ell,k} y_{j,\ell}^* \right] B_k(t) + \epsilon_j(t). \quad (4.7)$$

A simple way to obtain estimates for  $y_{j,\ell}^*$ ,  $\ell = 1, \dots, m$ ,  $j = 1, \dots, J$  is to use the estimated spectra  $\hat{\theta}_\ell$ , plug them into equation (4.7) and find which set of  $\mathbf{y}_j^*$  minimizes the square error of prediction, that is

$$\hat{\mathbf{y}}_j^* = \arg \min_{\mathbf{y}_j^*} \sum_{n=1}^T \sum_{\ell=1}^m \left( W_j^*(t_n) - y_{j,\ell}^* \hat{\theta}_\ell(t_n) \right)^2. \quad (4.8)$$

To assess the variance of such estimates, we use a leave-one-out jackknife technique.

1. For  $i = 1, \dots, I$ , leave out all data related to  $W_i(t)$  and find the estimate  $\theta_\ell^{(-i)}(t)$ . Then,
2. Use  $\hat{\theta}_\ell^{(-i)}(t)$  to “estimate”  $y_{i,\ell}$  as  $\hat{y}_{i,\ell}^{(-i)}$ .
3. Compare  $y_{i,\ell}$  with  $\hat{y}_{i,\ell}^{(-i)}$  using

$$S_\ell^2 = \frac{1}{I} \sum_{i=1}^I \left( y_{i,\ell} - \hat{y}_{i,\ell}^{(-i)} \right)^2$$

to estimate the variance of  $\hat{y}_{i,\ell}^{(-i)}$ .

4. For any new curve  $W_j^*(t)$  consider the confidence interval to be  $\hat{y}_{j,\ell}^* \pm cS_\ell$  (since the estimators are normally distributed conditionally on the calibration sample).

Notice that the normality of the estimators  $\hat{Y}_{j,\ell}^*$  is a consequence of assumption of the normality of the error processes  $\epsilon(t)$ . In our model, *cf.* expression (4.7),  $W_j^* = \hat{\theta}_0 + Ay_j^* + \epsilon^*$  where  $W_j^*$  is a  $(T \times 1)$  vector containing the  $j$ th prediction sample,  $\hat{\theta}_0$  is a  $(T \times 1)$  vector containing the values of  $\hat{\theta}_0(t_n)$  and  $A$  is a  $(T \times m)$  matrix formed by  $\hat{\theta}_c(t_n)$ . Since the calibration sample and the prediction sample are independent, the vectors  $W_j^*$ ,  $\hat{\theta}_0$  and  $A$  are independent. In this case, the estimator  $y_j^*$  given by (4.8) is

$$\hat{y}_j^* = (A'A)^{-1}A'(W_j^* - \hat{\theta}_0)$$

which is normally distributed conditionally on the calibration sample.

In order to compare the prediction performance of different approaches we are going to use the Standard Error of Prediction (SEP), which is the root mean square of the difference between the true and the predicted content. The contribution of component  $\ell$  is given by

$$\text{SEP}_\ell = \left( \frac{1}{J-1} \sum_{j=1}^J (y_{j,\ell}^* - \hat{y}_{j,\ell}^*) \right)^{1/2} \quad (4.9)$$



and the overall SEP is given by

$$\text{SEP} = \left( \frac{1}{mJ-1} \sum_{\ell=1}^m \sum_{j=1}^J (y_{j,\ell}^* - \hat{y}_{j,\ell}^*) \right)^{1/2}. \quad (4.10)$$

## 5 Artificial Datasets

We conducted a simulation study to assess the performance of the estimators proposed in Sections 3 and 4. The algorithm was implemented in R language (R Development Core Team, 2010) and is available upon request.

The wavelengths are arbitrarily ranging from 350 to 750 units, with sample points taken every 5 units. Two samples were simulated, one with  $I = 20$  curves and another including the 20 original observations and 80 additional ones, for a total  $I = 100$ . The samples were composed of  $m = 3$  analytes, with absorbances shown in Figure 1, and concentrations  $y_{i,1}, y_{i,2}, y_{i,3}$  randomly generated with a three-dimensional Dirichlet standard distribution ( $\alpha = 1$  for all dimensions). The concentrations were generated once and fixed afterwards, so they're accordingly treated as constants.

Two scenarios were considered for the covariance function of each constituent,  $\sigma_i(s, t) = \sigma^2 e^{-\phi|t-s|}$ , one with almost independent covariance structure for the analytes ( $\phi = 0.5$ ) and another one with  $\phi = 0.002$ , resulting in a very strong auto-correlation for the process. The variance was set to  $\sigma^2 = 4$  for both cases.

First we consider the results of a single experiment. The estimated analytes absorbance spectra  $\hat{\theta}_\ell(t)$ , and their true equivalents, are shown in Figures 1 (a) and (b). The mean residual sum of squares for the weakly correlated data is 3.88 when  $I = 20$  and 4.12 when  $I = 100$ ; for the strongly correlated data we have 2.61 when  $I = 20$ , and 3.53 when  $I = 100$ .

[Figure 1 here]

For the prediction step, the estimated standard deviations for the concentration estimators  $\hat{y}_1^*$ ,  $\hat{y}_2^*$  and  $\hat{y}_3^*$ , found via the leave-one-out estimation technique, are shown in Table 1. We can see that in this scenario the standard deviations for the strongly correlated data range from approximately 2 to 4 times the standard deviations of the weakly correlated data.

[Table 1 here]

The variance of the  $\hat{\mathbf{Y}}^*$  estimators, in the presence of strongly correlated errors, could be reduced if a generalized least squares method is implemented during the calibration step, as proposed by Dias, Garcia and Martarelli (2009). However, the high dimensionality of the problem and the fact that there is no replication of the data results in poor aggregated covariance estimates, with sample covariance matrices having high condition numbers and therefore often being numerically singular. To overcome this problem, we model the covariance function as suggested by Dias et al. (2012), we assumed that the covariance of each  $\epsilon_i(t)$  in model (2.4) is homogeneous and given by

$$\text{Cov}(\epsilon_i(s), \epsilon_i(t)) = \Sigma_i(s, t) = \sum_{\ell=1}^m y_{i,\ell}^2 \sigma_\ell^2 e^{-\phi_\ell |t-s|}.$$

We estimated the  $\phi_\ell$  and  $\sigma_\ell^2$  parameters using a least squares method on the observed sampled covariances, and then estimated  $\beta$  using

$$\hat{\beta} = (\mathbf{X}' \hat{\Sigma}^{-1} \mathbf{X})^{-1} \mathbf{X}' \hat{\Sigma}^{-1} \mathbf{W}, \quad (5.11)$$

with  $\mathbf{W}$ ,  $\mathbf{X}$  as defined in (3.6).

Now we replicate the experiment an additional 200 times, using the same configuration of  $\mathbf{y}$  for the calibration set, that is,  $y_{i,1}^*, y_{i,2}^*, y_{i,3}^*$  randomly generated with a three-dimensional Dirichlet standard distribution. We repeated the jackknife procedure and registered the estimated variances for the  $\hat{Y}_1^*$ ,  $\hat{Y}_2^*$  and  $\hat{Y}_3^*$  estimators, for the  $\phi = 0.5$  and  $\phi = 0.002$  cases. The simulation study compares several methods. The functional approaches consist of basis smoothing method when  $K = 14$  using ordinary least squares estimation (OLS-K), basis smoothing method with generalized least squares estimation proposed in Dias et al. (2012) (GLS-K) and Smoothing Splines method with tuning parameter  $\lambda$  optimizing the GCV criteria (OLS-SS). For the classical multivariate methods, we also offer jackknife estimates for Multiple Linear Regression (MLR), Principal Components Regression using either 3 components (PCR-o, from oracle, as the true calibration curves have about three distinguishable features in the principal components sense), or explaining 90% of the sample variability of the data (PCR-p, from proportion) and Partial Least Squares case (PLS-o, PLS-p, using the same number of components as in the Principal Components Regression).

The median and interquartile range (IQR) results are given in Table 2. Notice that the theoretical value of all the standard deviations is  $\sqrt{1/18} \approx 0.24$  (since the values were generated

using a standard Dirichlet distribution). We can see that increasing the number of sampled curves has little effect on the precision of the estimators. On the other hand, in agreement with the preliminary results shown in Table 1, having a strongly correlated scenario for the sampling errors seems to produce less precise estimators. Our methods are overall better than Multiple Linear Regression (MLR) but do not show the same degree of optimality as the Principal Components and Partial Least Squares methods. We emphasize that PCR/PLS methods, on the other hand, do not provide estimates of the curves  $\theta$  and are unable to separate the aggregated curves for each analyte.

[Table 2 here]

To get estimates of both the bias and variability at prediction of new values, we ran a second experiment on the following  $\mathbf{Y}^*$

$$\mathbf{Y}^* = \begin{pmatrix} 0.4 & 0.1 & 0.5 \\ 0.2 & 0.3 & 0.5 \\ 0.1 & 0.4 & 0.5 \\ 0.5 & 0.4 & 0.1 \end{pmatrix}$$

First, we generated 40 independent learning sets, in which we performed the calibration step using five models: K-basis spline with ordinary least squares (OLS-K), smoothing spline with  $\lambda$  minimizing GCV (OLS-SS), multiple linear regression (MLR), principal components regression and partial least squares with a number of components explaining 90% of data variability (PCR-p and PLS-p, respectively). For each of those 40 independent calibration sets, we generated 5 independent curves  $W_j^*(t)$  with concentrations based on  $\mathbf{Y}^*$  to be used for prediction purposes. Then, we predict  $\hat{Y}_1^*$ ,  $\hat{Y}_2^*$  and  $\hat{Y}_3^*$ . Indexing the 40 calibration sets with  $g$  and the 5 replicates with  $h$ , we can estimate both the variability (V) and the squared bias ( $B^2$ ) using

$$V_c = \sum_{g=1}^{40} \sum_{h=1}^5 (\hat{Y}_{gh,c} - \bar{\hat{Y}}_{g,c})^2$$

and

$$B_c^2 = \sum_{g=1}^{40} \sum_{h=1}^5 (Y_{gh,c} - \bar{Y}_{g,c})^2.$$

The results of the prediction test for new, independent samples is shown in Table 3. One striking feature is how much bias is introduced in all procedures when high correlation is present. In this case, the fixed K-basis and smoothing splines are comparable; both perform better than Multiple Linear Regression but have lower accuracy and precision than Principal Components Regression and Partial Least Squares. Again, we stress the fact that these last two methods do not offer estimates of the individual absorption spectrum for each constituent, thus being better when prediction is the sole interest of the experimenter. Furthermore, another shortcoming of these multivariate procedures is that they cannot be applied at all if the spectra are measured at different wavelengths.

[Table 3 here]

## 6 Real Datasets

### 6.1 PAH data

The sample consists of 50 chemical samples of 10 polyaromatic hydrocarbons (PAH) obtained by Electronic Absorption Spectroscopy, each sample is composed of varying compositions of 10 different constituents (pyrene, acenaphthene, anthracene, acenaphthylene, chrysene, benzanthracene, fluoranthene, fluorene, naphthalene, phenanthracene). Each sample was submitted to 27 wavelengths (220nm–350nm). This dataset was presented by Brereton (2003) to illustrate multivariate calibration and prediction techniques.

This dataset is divided into two sets, 25 curves prepared to achieve an orthogonal design with 5 levels of concentration for each constituent to be used as a calibration sample. The other 25 curves have the same five concentration levels for each constituent and can be used for prediction purposes. One peculiarity of this dataset is that the concentration is not given in percentage but in mg/l. This has no effect in our estimation scheme. Notice that pyrene, chrysene, benzanthracene, fluorene and phenanthracene have generally higher concentrations than the other analytes.

Figure 2 compares the estimated analytes spectra ( $\hat{\theta}_\ell(t), \ell = 1, \dots, 10$ ) for the two proposed basis expansion approaches. For this case, we used ordinary least squares without any assumption on the covariance structure. The Smoothing Spline estimates are less smooth and have

more “bumps”. Hence, it captures more of the local variation of the data. This is expected and, for this dataset, a desirable property. As pointed by Brereton (2003), the curves are sampled at a coarse grid of wavelengths and this causes the noise to be reduced. Therefore, most of the local variation in the curves are important features of the data and need to be captured. Figure 3 presents the fit for 4 chemical samples suggesting that our model provides excellent fits to the observed aggregated data.

[Figure 2 here]

[Figure 3 here]

Notice that the fitted values using the Smoothing Splines are much closer to the observed curves than the ones obtained via Basis Smoothing. Finally, the leave-one-out technique for variance estimation of the predicted curves is employed, and the results are shown in Table 7. We remark that the estimated variances are similar in both methods.

[Table 7 here]

Of course, we aim not only for a fit with small residuals but with high prediction power. Now Figure 4 shows the  $y_\ell^*$ ,  $\ell = 1, \dots, 10$  for all the analytes for the 25 curves in the independent test set (Brereton, 2003, Table 5.20), against their predicted concentration for the model based on our procedures. The dashed lines show where an exact prediction would be. In general, both procedures have a similar performance in terms of prediction. In fact, for benzanthracene, the constituent that has the largest concentration for all the chemical samples (with percentages ranging from 13.7% to 59.6%) both procedures have highly predictive power. Other constituents that present relatively high concentrations are: pyrene, chrysene, fluorene and phenanthracene. We present the SEP (mg/l) for each component and the overall SEP in Table 5, and again we provide a comparison with the MLR, PCR and PLS methods (we choose 10 components after Brereton, 2003). We stress that the smoothing spline is capable of obtaining good predictions even when the respective concentrations are not particularly high, see for example anthracene.

[Table 5 here]

[Figure 4 here]

## 6.2 Tecator data

These data are recorded on a Tecator Infratec Food and Feed analyzer working in the wavelength range 850 – 1050 nm by the Near Infrared Transmission (NIT) principle. The data are made available as a benchmark for regression models and it is available in the public domain with no responsibility from the original data source from Tecator<sup>1</sup> Each sample contains finely chopped pure meat with different moisture, fat and protein contents. The task is to predict the fat content of a meat sample on the basis of its near infrared absorbance spectrum.

For each meat sample the data consists of a 100 channel spectrum of absorbances and the contents of moisture (water), fat and protein. The three contents, measured in percent, were determined by analytic chemistry. Figure 5 shows paired scatterplots for the concentrations of moisture, fat and protein. It's important to emphasize the regions for prediction of  $\mathbf{y}$  values outside of these clouds will be, in some sense, *extrapolations* and consequently have very large prediction errors.

[Figure 5here]

There are 240 samples, further described by Borggaard and Thodberg (1992), divided into 5 data sets for the purpose of model validation and extrapolation studies; the training set consisting of 129 samples, the monitoring dataset consisting of 43 samples, the testing dataset consisting of 43 samples, the extrapolation set for fat content with 8 samples and the extrapolation set for protein content with 17 samples.

The spectra are preprocessed using a principal component analysis on the data set C, and the first 22 principal components (scaled to unit variance) are included for each sample in the dataset. We did not, however, use this preprocessed data to calibrate our fit.

Figure 6 shows the absorbance spectra estimated with the Calibration plus Monitoring sub-dataset for the Moisture, Fat and Protein components. Notice here the smoothing spline seems to capture some local features that are over smoothed when the number of basis is kept fixed, particularly in the Fat component at wavelengths 920 to 990, approximately. If we observe carefully the data, there is some important feature to be captured in the curves at this part of the spectrum. However we choose not to use GCV to find  $\lambda$ , as the optimal value provided by it

---

<sup>1</sup><http://lib.stat.cmu.edu/datasets/tecator>. The data can be redistributed as long as this permission note is attached.

( $\lambda = 33500$ ) oversmoothed the Protein component and had consequently a worse performance in the prediction step, in terms of SEP. We decided to pick  $\lambda = 330$  by inspecting plots of the estimated curves (like Figure 6) until a satisfactory degree of smoothness was found.

[Figure 6 here]

Inspecting the residuals, we may see the errors probably fit the strongly correlated data scenario. From the simulation conducted in Section 5 we expect the overall prediction error to be greater than if we had a weakly correlated noise.

Now Figure 7 shows the  $y_1^*$ ,  $y_2^*$  and  $y_3^*$  values of moisture, fat and protein – respectively – for the Testing data, against their predicted concentrations for the model based on our procedure. Figure 7 shows that both methods, fixed basis smoothing and smoothing splines, have similar prediction power. The dashed lines shows where an exact prediction would lie, so the given standard deviation estimates (Table 6) seem appropriate.

[Figure 7 here]

[Table 6 here]

Comparing the true values for the training data with their predicted correspondents, we find that the Standard Error of Prediction for the fat component on the prediction data set is equal to 0.102 using smoothing splines method. Table 7, originally taken from Eilers et al. (2009) but modified to include our results, show the SEP results for neural networks (see Borggaard and Thodberg, 1992; Thodberg, 1995). For instance, our method is roughly 3.5 times more efficient than the 13-X-1 network in the prediction sense.

[Table 7 here]

## 7 Concluding remarks

In this work we propose to use a functional approach to analyze NIR spectroscopy data. The main novelty of this work is to use a functional version of the Beer-Lambert formula so that the calibration procedure can be interpreted as modeling latent (disaggregated) mean curves when we only have available observations of the population (aggregated) curves. We considered

two procedures for estimation of the latent curves, basis smoothing and smoothing splines. In general, smoothing splines capture more of the local variation of the data and produce less smooth estimates. Once the calibration procedure is performed, prediction was made by minimizing the squared error of prediction. To assess the variance of such estimates, we used an idea based on the leave-one-out jackknife technique.

To show the strength of the proposed functional approach, we analyzed artificial datasets generated from the different correlation structures and two examples with data available in the literature. We compared our method with the most common methods available in the literature, multiple linear regression (MLR), principal component regression (PCR) and partial least squares (PLS). As a measure of fit we used the Standard Error of Prediction (SEP) which is the root mean squared difference between predictions and reference values. In all cases, the fixed K-basis and smoothing splines are comparable; both perform better than MLR but sometimes they have lower accuracy and precision than the PCR and PLS. On the other hand, the functional approach has two main advantages over these multivariate methods: i) it can be applied if the spectra are measured at distinct wavelengths for distinct curves; ii) it provides estimates for the individual absorption curves for each constituent. Moreover, the analysis of the artificial datasets demonstrates the impact of the temporal correlation in the calibration and prediction steps showing the need to model the correlation structure.

The applicability of our approach can also be viewed through the future developments, already under work, which include:

- (i) Implement Functional Principal Components or other dimensionality reduction techniques to improve the performance of the functional approach with respect to prediction only;
- (ii) Perform jointly estimation of the calibration curves and predicted concentration values;
- (iii) Consider the case of outlier prediction in cases where the prediction sample is inconsistent with the calibration data.

**Acknowledgments** The authors would like to thank Prof. John Rice, U. C. Berkeley for many fruitful discussions. This work was partially funded by CNPq grants 302755/2010-1, 476764/2010-6, 302182/2010-1 and 553438/2009-3. The authors are grateful to Department of Mathematics of the University of Wisconsin-Madison and Department of Statistics of the University of California, Berkeley, for their hospitality.



## References

- Alsberg, B. (1993). Representation of spectra by continuous functions, *Journal of Chemometrics* **7**: 177–193.
- Aneiros-Pérez, G. and Vieu, P. (2006). Semi-functional partial linear regression, *Statistics & Probability Letters* **76**(11): 1102 – 1110.
- Borggaard, C. and Thodberg, H. H. (1992). Optimal minimal neural interpretation of spectra, *Analytical Chemistry* **64**: 545–551.
- Brereton, R. G. (2003). *Chemometrics: Data Analysis For the Laboratory and Chemical Plant*, John Wiley & Sons, Chichester.
- Burns, D. A. and Ciurczak, E. W. (2007). *Handbook Of Near-infrared Analysis*, CRC PRESS.
- Davis, T. (2000). NIR: A Combination of Spectroscopies. Course notes.
- de Boor, C. (1978). *A Practical Guide to Splines*, Springer Verlag, New York.
- Dias, R. (1999). Sequential adaptive non parametric regression via H-splines, *Communications in Statistics: Computations and Simulations* **28**: 501–515.
- Dias, R., Garcia, N. L. and Martarelli, A. (2009). Non-parametric estimation for aggregated functional data for electric load monitoring, *Environmetrics* **20**(2): 111–130.
- Dias, R., Garcia, N. L. and Schmidt, A. (2012). A hierarchical model for aggregated functional data, *to appear in Technometrics* .
- Eilers, P. H. C., Li, B. and Marx, B. D. (2009). Multivariate calibration with single-index signal regression, *Chemometrics and Intelligent Laboratory Systems* **96**: 196–202.
- Ferraty, F. and Vieu, P. (2006). *Nonparametric functional data analysis: theory and practice*, Springer series in statistics, Springer.
- Jørgensen, B. and Goegebeur, Y. (2007). Multivariate data analysis and chemometrics, Course notes.  
**URL:** <http://statmaster.sdu.dk/courses/ST02>

- Kooperberg, C. and Stone, C. J. (1991). A study of logspline density estimation, *Comp. Stat. Data Anal.* **12**: 327–347.
- R Development Core Team (2010). *R: A Language and Environment for Statistical Computing*, R Foundation for Statistical Computing, Vienna, Austria. ISBN 3-900051-07-0.  
**URL:** <http://www.R-project.org>
- Ramsay, J. O. and Silverman, B. W. (2005). *Functional Data Analysis, Second Edition*, Springer-Verlag, New York.
- Saeys, W., De Ketelaere, B., and Darius, P. (2008). Potential applications of functional data analysis in chemometrics, *J. Chemometrics* **22**: 335344.
- Shenk, J. S. and Westerhaus, M. O. (1991). New standardization and calibration procedure for nir analytical systems, *Crop Science* **31**: 1692–1694.
- Siesler, H. W., Ozaki, Y., Kawata, S. and Heise, H. M. (2002). *Near-Infrared Spectroscopy: Principles, Instruments, Applications*, Wiley-VCH, Weinheim.
- Silverman, B. W. (1986). *Density Estimation for Statistics and Data Analysis*, Chapman and Hall (London).
- Thodberg, H. H. (1995). A review of bayesian neural networks with an application to near infrared spectroscopy, *IEEE Transactions on Neural Networks* **7**: 56–72.
- Vidakovic, B. (1999). *Statistical Modeling by Wavelets*, Wiley Series in Probability and Statistics: Applied Probability and Statistics, John Wiley & Sons Inc., New York. A Wiley-Interscience Publication.
- Wahba, G. (1990). *Spline Models for Observational Data*, SIAM, Philadelphia.

	Weakly Correlated		Strongly Correlated	
	$I = 20$	$I = 100$	$I = 20$	$I = 100$
$S_1$	0.020	0.016	0.061	0.061
$S_2$	0.027	0.024	0.042	0.055
$S_3$	0.022	0.021	0.058	0.063

Table 1: Estimated standard deviations for the  $\hat{y}_1^*$ ,  $\hat{y}_2^*$  and  $\hat{y}_3^*$ , using the jackknife procedure

$\phi$	I	C	OLS-K	GLS-K	OLS-SS	MLR	PCR-o	PCR-p	PLS-o	PLS-p
0.5	20	1	1.8 (0.4)		1.9 (0.5)	2.0 (0.4)	1.9 (0.4)	1.9 (0.5)	2.0 (0.5)	2.0 (0.6)
		2	2.5 (0.6)		2.6 (0.6)	2.8 (0.6)	2.9 (0.6)	2.9 (0.8)	3.0 (0.8)	3.1 (1.0)
		3	2.1 (0.5)		2.1 (0.5)	2.2 (0.5)	1.8 (0.4)	1.8 (0.5)	1.8 (0.4)	1.9 (0.6)
		*	<b>2.1 (0.7)</b>		<b>2.2 (0.7)</b>	<b>2.3 (0.7)</b>	<b>2.0 (0.9)</b>	<b>2.1 (0.9)</b>	<b>2.1 (1.0)</b>	<b>2.2 (1.0)</b>
	100	1	1.7 (0.2)		1.7 (0.2)	1.8 (0.2)	1.6 (0.2)	1.9 (0.2)	1.7 (0.2)	3.7 (0.9)
		2	2.3 (0.2)		2.3 (0.2)	2.3 (0.2)	2.3 (0.2)	2.7 (0.4)	2.6 (0.3)	5.3 (1.5)
		3	1.8 (0.2)		1.9 (0.2)	1.9 (0.2)	1.5 (0.2)	1.8 (0.2)	1.6 (0.2)	3.6 (0.8)
		*	<b>1.9 (0.5)</b>		<b>1.9 (0.5)</b>	<b>1.9 (0.5)</b>	<b>1.7 (0.7)</b>	<b>2.0 (0.8)</b>	<b>1.8 (0.8)</b>	<b>4.0 (1.5)</b>
0.002	20	1	6.7 (1.5)	6.6 (1.5)	6.9 (1.6)	6.9 (1.6)	4.3 (1.0)	4.3 (1.0)	4.3 (1.0)	4.3 (1.0)
		2	5.4 (1.5)	5.4 (1.4)	5.6 (1.6)	5.6 (1.6)	4.3 (1.0)	4.3 (1.0)	4.3 (1.0)	4.3 (1.0)
		3	7.5 (2.1)	7.3 (2.0)	7.7 (2.2)	7.7 (2.2)	3.7 (0.9)	3.7 (0.9)	3.7 (0.9)	3.7 (0.9)
		*	<b>6.5 (2.0)</b>	<b>6.5 (1.9)</b>	<b>6.7 (2.0)</b>	<b>6.7 (2.0)</b>	<b>4.0 (1.1)</b>	<b>4.1 (1.1)</b>	<b>4.1 (1.1)</b>	<b>4.1 (1.1)</b>
	100	1	6.1 (0.6)	6.1 (0.6)	6.1 (0.7)	6.1 (0.7)	3.7 (0.4)	3.6 (0.3)	3.7 (0.4)	3.7 (0.4)
		2	5.0 (0.5)	5.1 (0.6)	5.1 (0.5)	5.1 (0.5)	3.8 (0.4)	3.8 (0.4)	3.8 (0.4)	4.0 (0.5)
		3	7.0 (0.6)	6.9 (0.7)	7.0 (0.7)	7.0 (0.7)	3.3 (0.3)	3.2 (0.3)	3.3 (0.3)	3.3 (0.4)
		*	<b>6.1 (1.5)</b>	<b>6.1 (1.5)</b>	<b>6.1 (1.5)</b>	<b>6.1 (1.5)</b>	<b>3.6 (0.5)</b>	<b>3.6 (0.5)</b>	<b>3.6 (0.5)</b>	<b>3.6 (0.6)</b>

Table 2:  $10^2$  times Median ( $10^2$  times IQR) of 200 independent standard deviation simulation estimates for the  $\hat{Y}_1^*$ ,  $\hat{Y}_2^*$  and  $\hat{Y}_3^*$  estimators, using the jackknife procedure. OLS-K: fixed 14 spline basis with ordinary least squares; GLS-K: fixed 14 spline basis with generalized least squares (only for  $\phi = 0.002$ ); OLS-SS: smoothing spline ( $\lambda$  minimizing GCV); MLR: multiple linear regression; PCR-o, PLS-p: Principal Components Regression with either 3 components selected or with  $p$  components that explain 90% of observed curves variability; PLS-o, PLS-p: Partial Least Squares, same number of components as corresponding PCR. True standard deviation =  $2.4 \times 10^{-2}$

	OLS-K		OLS-SS		MLR		PCR		PLS	
	B <sup>2</sup>	V	B <sup>2</sup>	V	B <sup>2</sup>	V	B <sup>2</sup>	V	B <sup>2</sup>	V
I = 20	0.13	0.38	0.14	0.37	0.14	0.36	0.13	0.34	0.14	0.40
I = 20, correlated	1.33	3.26	1.33	3.26	1.36	3.32	0.45	1.26	0.45	1.26
I = 100	0.08	0.30	0.08	0.30	0.08	0.30	0.10	0.33	0.42	1.35
I = 100, correlated	0.79	2.81	0.79	2.81	0.80	2.89	0.23	0.97	0.24	1.03

Table 3:  $10^3$  times estimated squared bias and variability of the prediction set, for all components added up: OLS-K: fixed K=14 spline basis with ordinary least squares; OLS-SS: smoothing spline with  $\lambda$  minimizing GCV; MLR: multiple linear regression; PCR: Principal Components Regression with  $p$  components that explain 90% of observed curves variability; PLS: Partial Least Squares, same number of components as PCR.

Constituent	Basis Smoothing (OLS-K)	Smoothing Splines (OLS-SS)
Pyrene	0.06	0.05
Acenaphthene	0.04	0.07
Anthracene	0.11	0.04
Acenaphthylene	0.41	0.42
Chrysene	0.28	0.27
Benzanthracene	1.64	1.64
Fluoranthene	0.41	0.41
Fluorene	0.59	0.56
Naphthalene	0.11	0.11
Phenanthracene	0.49	0.36

Table 4: Leave-one-out Standard Deviation estimates (mg/l) for PAH data.

Constituent	OLS-K	OLS-SS	MLR	PCR	PLS
Pyrene	0.09	0.09	0.09	0.09	0.09
Acenaphthene	0.05	0.06	0.06	0.03	0.03
Anthracene	0.11	0.04	0.03	0.03	0.03
Acenaphthylene	0.08	0.09	0.09	0.06	0.06
Chrysene	0.10	0.06	0.06	0.05	0.04
Benzanthracene	0.06	0.07	0.07	0.07	0.06
Fluoranthene	0.10	0.09	0.09	0.08	0.08
Fluorene	0.32	0.23	0.24	0.20	0.15
Naphthalene	0.03	0.04	0.04	0.03	0.04
Phenanthracene	0.31	0.09	0.08	0.09	0.08
Overall	0.16	0.10	0.11	0.09	0.08

Table 5: Standard Error of Prediction (mg/l) for PAH data. OLS-K: fixed-K (14) spline basis with ordinary least squares; OLS-SS: smoothing spline ( $\lambda$  minimizing GCV); MLR: multiple linear regression; PCR: Principal Components Regression with 10 components (Brereton, 2003); PLS: Partial Least Squares, same number of components as PCR.

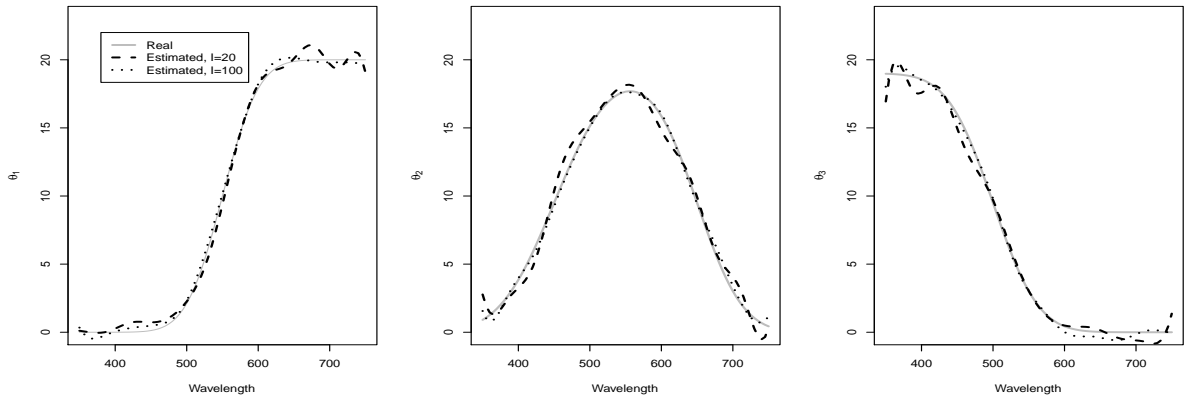
Component $\ell$	OLS-K		OLS-SS	
	$S_\ell$	SEP $_\ell$	$S_\ell$	SEP $_\ell$
Moisture	0.386	0.081	0.386	0.080
Fat	0.514	0.106	0.513	0.102
Protein	0.159	0.040	0.159	0.039
Overall		0.081		0.077

Table 6: Prediction  $S_\ell$  estimates and SEP for individual components. OLS-K: fixed K=14 spline basis with ordinary least squares; OLS-SS: smoothing spline with  $\lambda$  minimizing GCV.

Method	SEP
10-6-1 network, early stopping	0.650
10-3-1 network, Bayesian	0.520
13-X-1 network, Bayesian, Automatic Relevance Determination	0.360
Basis Smoothing	0.106
Smoothing Spline	0.102

Table 7: Table summarizing the prediction error for fat in the Tecator data, compared to a neural network approach; first three entries are tabulated data available with Tecator dataset.

(a)



(b)

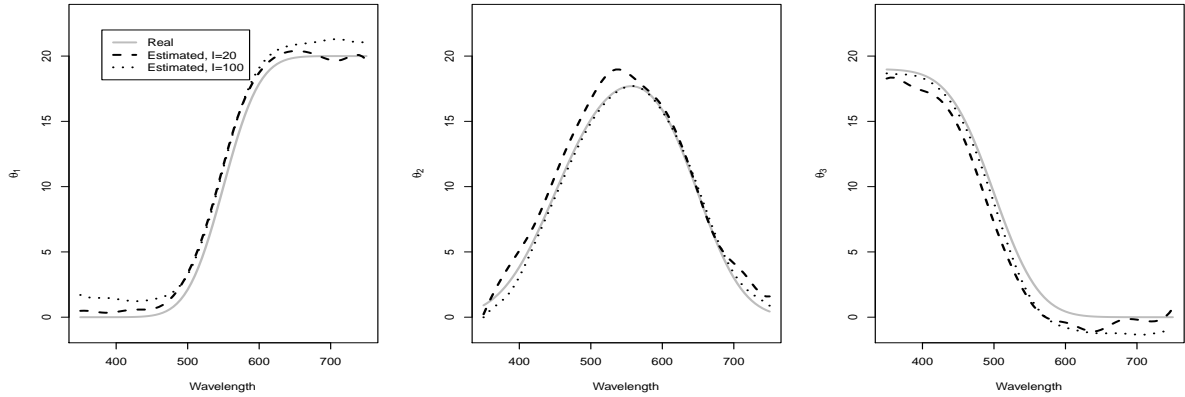


Figure 1: Estimated absorbance spectra,  $\hat{\theta}_1(t)$ ,  $\hat{\theta}_2(t)$  and  $\hat{\theta}_3(t)$ , for (a) weakly correlated scenario and (b) strongly correlated scenario, using fixed  $K$  basis. The dashed lines represent the spectra obtained when the number of sampled curves is  $I = 20$ , whereas the dotted lines represent the estimated spectra when  $I = 100$ .

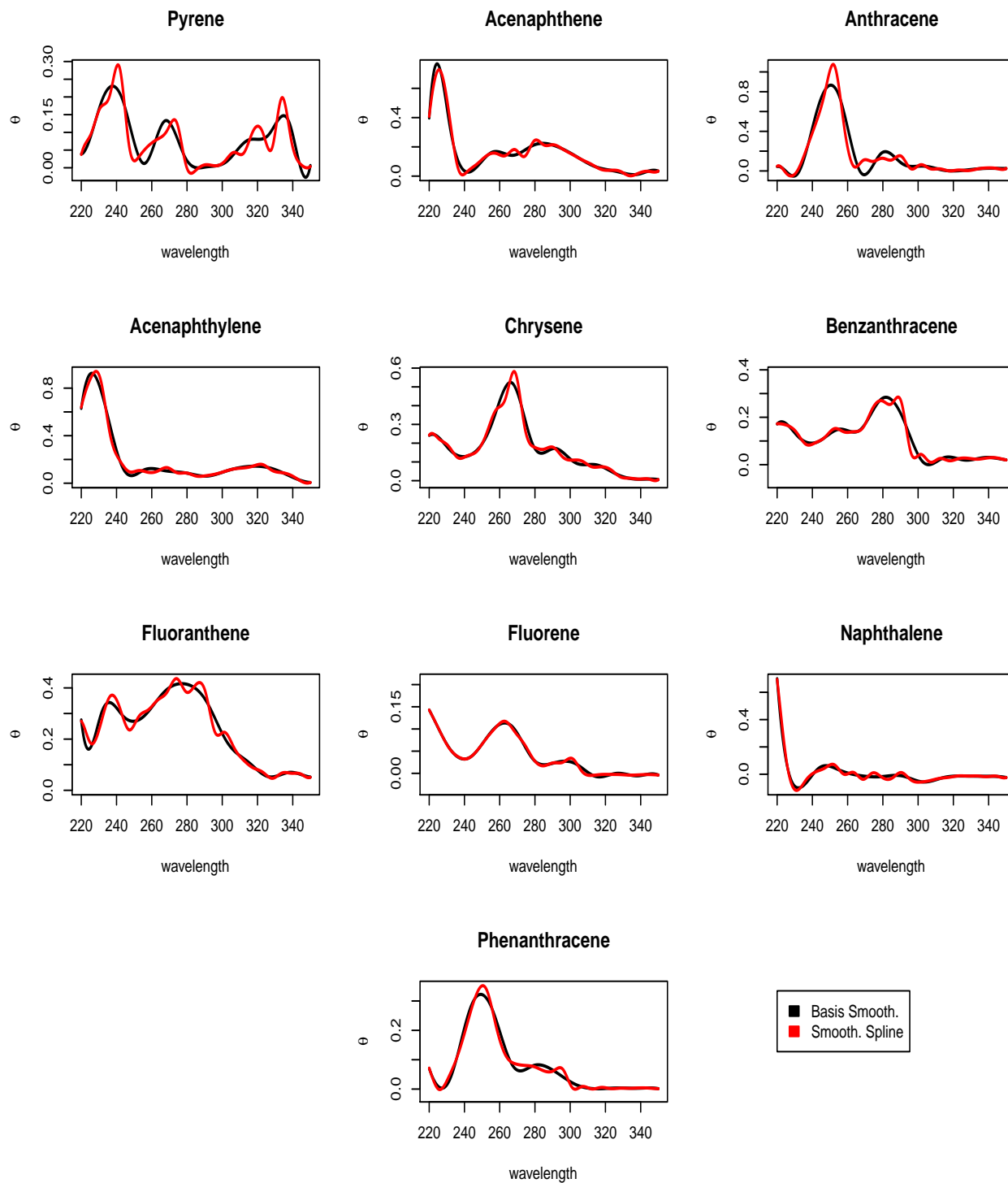


Figure 2: Estimated absorbance spectra  $\hat{\theta}_\ell$ ,  $\ell = 1, \dots, 10$  for PAH dataset



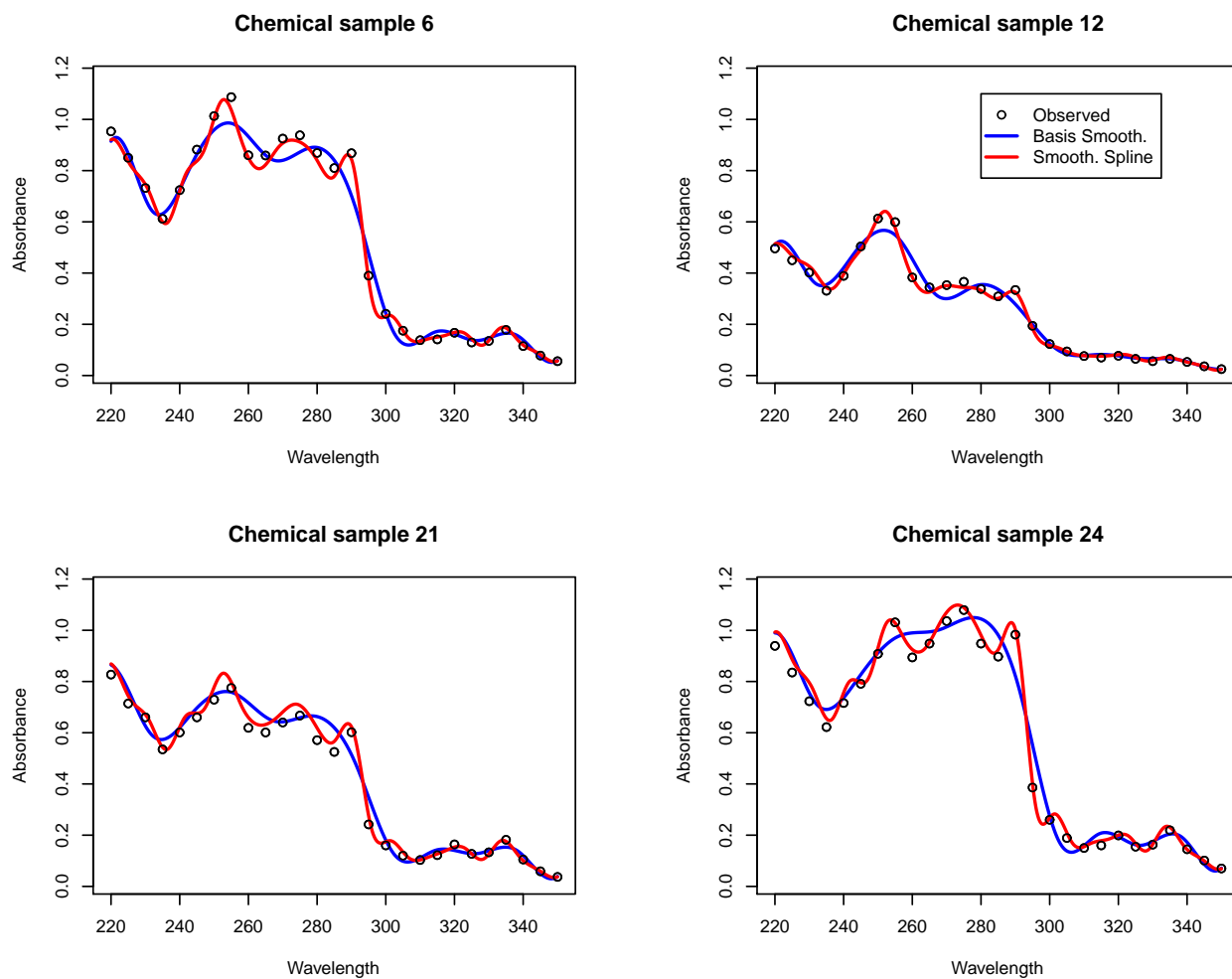


Figure 3: Estimated aggregated curves  $(\sum_{\ell=1}^m y_{i\ell}\hat{\theta}_{\ell}(t))$  for chemical samples  $i=6,12, 21$  and  $24$ .

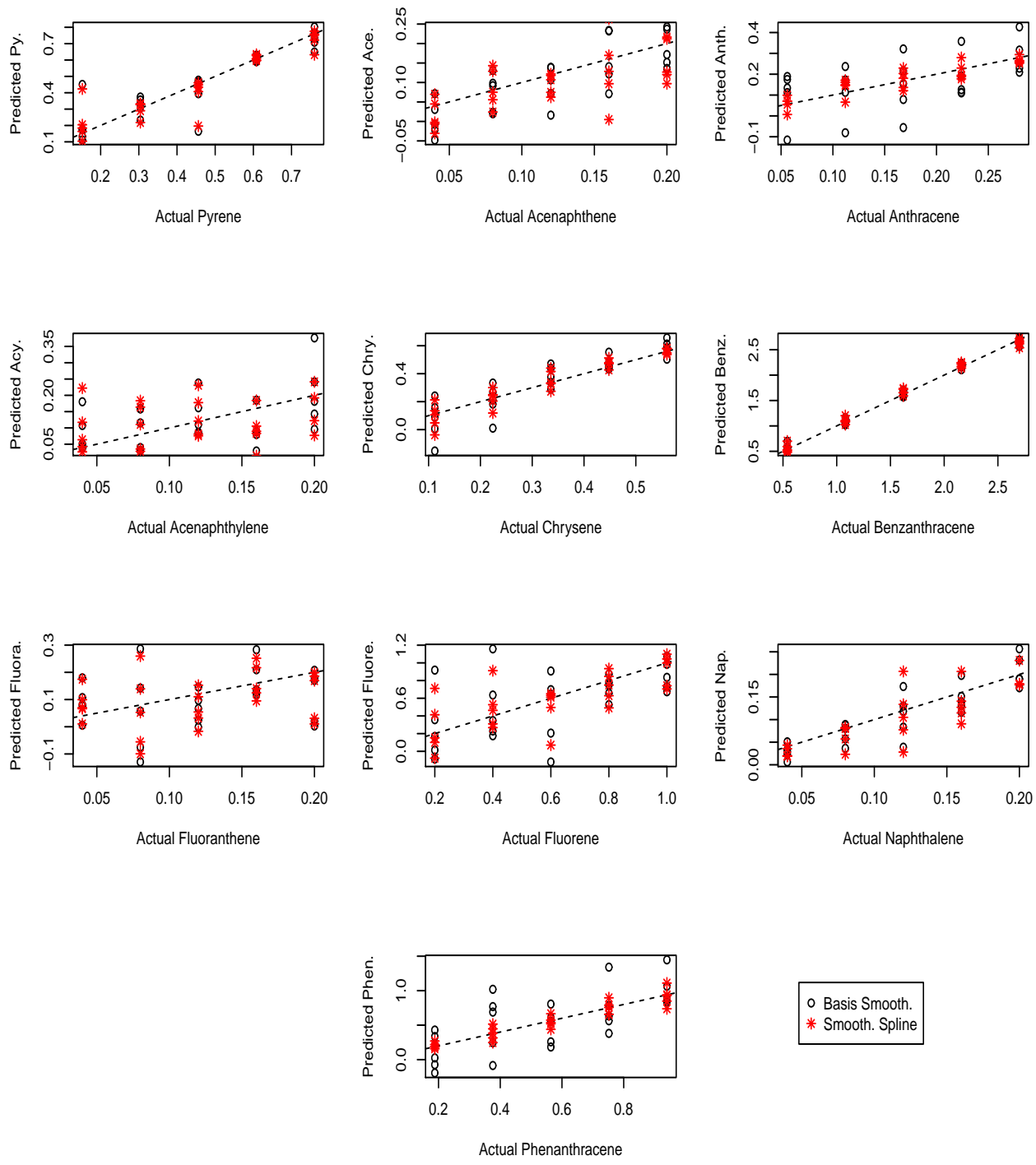


Figure 4: The predicted values  $\hat{y}$  for the Independent Test Set, for pyrene, acenaphthene, anthracene, acenaphthylene, chrysene, benzanthracene, fluoranthene, fluorene, naphthalene, phenanthracene and their predicted values.

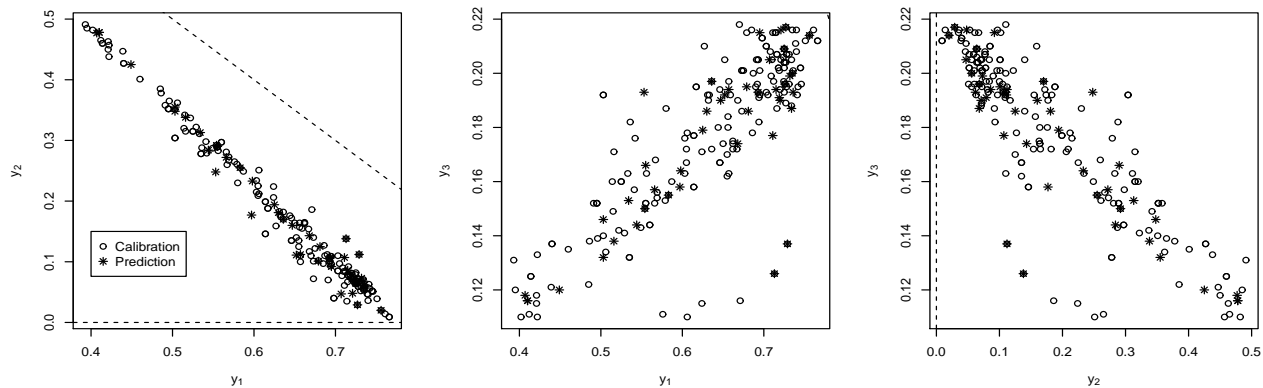


Figure 5: Pairwise concentration values for moisture, fat and protein for the Tecator data

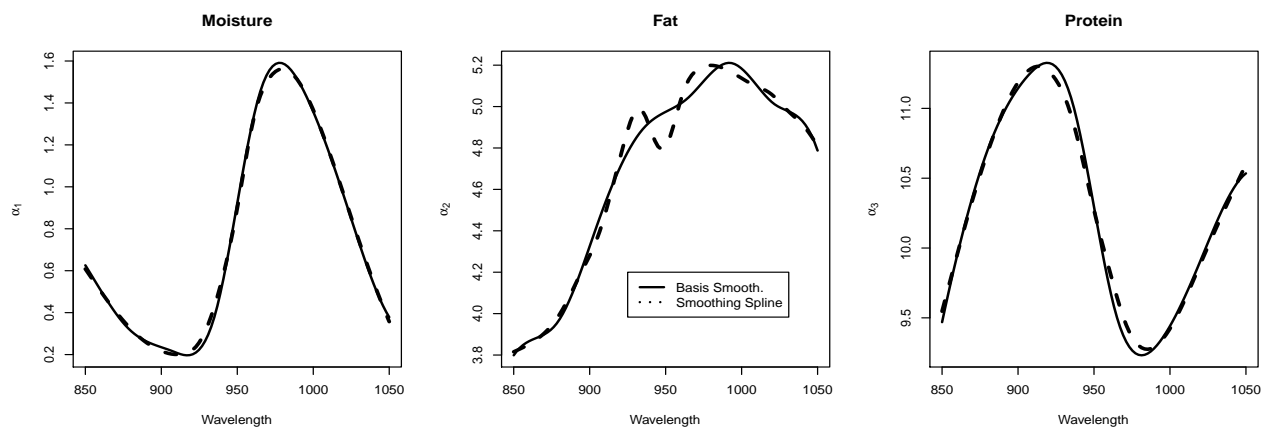


Figure 6: Tecator estimated absorbance spectra  $\hat{\theta}_1$ ,  $\hat{\theta}_2$  and  $\hat{\theta}_3$

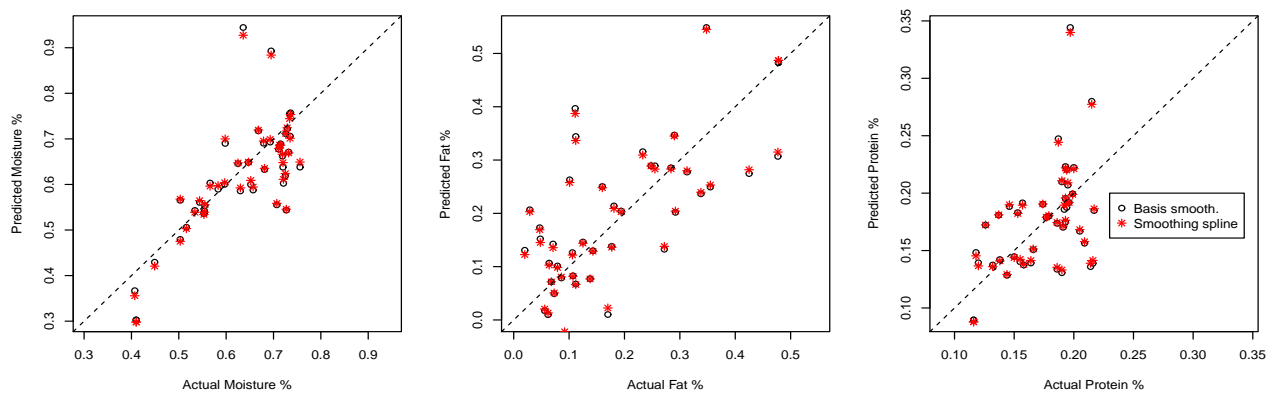


Figure 7: The  $y$  values for the Testing Data, for moisture, fat and protein, and their predicted values.